Situation-Aware Feedback-Predictive Control Framework for Lane-Less Dense Traffic

Parthib Khound[1], Nishant Jayesh Bhave[1], Siyang Xie[2], and Debraj Chakraborty[1]

***Abstract*— Navigating dense, lane-less traffic remains one of the most challenging scenarios for autonomous vehicles, especially in emerging regions where road structure and driver behavior are highly unpredictable. This paper presents a hybrid control framework tailored for such environments, integrating a 360° zone-based perception module with a dual-layer control strategy that combines classical feedback and predictive optimization. The longitudinal feedback controller computes reference speed based on braking distance and steering dynamics, while the lateral controller tracks a virtual optimal lane derived from the spatial distribution of neighboring vehicles. The predictive planner samples control inputs over a time horizon and selects the most feasible trajectory using a multi-term cost function. Simulation results across diverse one-way traffic scenarios demonstrate the framework's robustness, responsiveness, and suitability for unstructured traffic. As an initial structured approach of designing autonomous driving for lane-less traffic environment, the work illustrates the potential of hybrid control strategies while indicating the need for further nonlinear stability analysis and broader validation in future studies.**

***Index Terms*— lane-less traffic, automated driving, predictive vehicle control, vehicle trajectory planning, feedback-predictive control.**

I. Introduction

Advanced driver assistance systems (ADAS) aim to improve road safety by reducing human error [1]. Most current ADAS technologies are developed for structured road networks and regulated traffic conditions. Adaptive cruise control (ACC) and lane keeping systems (LKS) are common examples, handling longitudinal and lateral vehicle control respectively [2]. Platooning control systems further extend longitudinal coordination by optimizing car-following maneuvers [3]. Applying these technologies to unstructured traffic environments, such as those found in emerging countries like India, poses significant challenges due to inconsistent lane discipline and, in many cases, poorly defined or absent lane markings.

Automated driving in dense, unstructured traffic environments, where lane markings are absent or disregarded, has gained increasing attention over recent years. These conditions challenge conventional lane-based planning and control frameworks and have led to the development of alternative approaches that attempt to capture the complexity of such traffic. For instance, the flexible car–following model proposed by [4] focuses on longitudinal control in heterogeneous traffic using multi-leader logic. It allows a vehicle to respond to multiple leaders ahead, improving adaptability in weak lane discipline scenarios. The model is calibrated using real-world trajectory data from India and emphasizes data-driven modeling. However, it does not explicitly address lateral motion or vehicle actuation constraints such as steering and throttle, limiting its applicability to full-motion planning in lane-less traffic environments.

In [5], a microscopic model is introduced for lane-less traffic, inspired by human driving behavior in congested traffic. It uses a graph-theoretic influence framework to simulate both lateral and longitudinal interactions. Vehicles are modeled as point masses, and lateral motion is treated as direct drift, decoupled from longitudinal control. Each vehicle is influenced by its neighbors based on proximity and angle, and the model assumes that all vehicles obey a common control law. This offers a very structured way to simulate collective behavior. However, as the proposed method is inspired from human driving, it overlooks the critical role of human error, which is widely recognized as the leading cause of road accidents [6]. Furthermore, by assuming uniform compliance and a point-mass model, the model fails to capture the variability and unpredictability inherent in real-world traffic, limiting its applicability to autonomous driving systems operating in unstructured environments.

In [7], a macroscopic model is proposed that treats traffic as a compressible fluid, enabling nudging interactions among connected automated vehicles (CAVs). Vehicles are not bound to lanes and influence others ahead through sensing or communication, conceptually resembling pressure in fluid dynamics. While effective in structured CAV networks, the model assumes centralized coordination and cooperative behavior, which is not feasible for ego-vehicle autonomy in mixed traffic. It does not model individual vehicle control inputs such as steering or throttle and relies on emergent behavior from collective interactions.

More recently, [8] analyzed traffic stability under weak lane discipline by incorporating reaction time distribution into a hexagonal vehicle formation framework. This method offers insights into collective dynamics and stability margins in idealized traffic configurations. The formation-based approach is designed for theoretical analysis and assumes equilibrium conditions, making it unsuitable for decentralized, ego-centric planning in unstructured traffic where individual vehicles must respond autonomously to unpredictable local

[1]P. Khound, N. J. Bhave, and D. Chakraborty are with the Department of Electrical Engineering, Indian Institute of Technology Bombay, Mumbai-400076, India (e-mail: khound@ee.iitb.ac.in, nishant.bhave@iitb.ac.in, and dc@ee.iitb.ac.in).

[2]S. Xie is with Innovative Research Excellence, Honda R&D Co., Ltd., Tokyo 105-0001, Japan (e-mail: siyang_xie@jp.honda).

interactions.

In [9], a reinforcement learning framework is proposed where multiple autonomous vehicles optimize traffic flow through policy learning and coordination. The approach assumes vehicle-to-vehicle communication and shared policies. While the control system is not explicitly modeled, the learned policies operate over steering and throttle commands. However, the paper does not describe fallback mechanisms or analyze robustness under unpredictable traffic conditions, which are important considerations for deployment in mixed environments.

Other studies, such as those analyzing overtaking behavior [10] and vehicle detection in lane-less traffic [11], offer insights into behavioral and perception modeling for lane-less environment, respectively. For example, the overtaking decision model [10] uses a probabilistic framework based on lateral and longitudinal positions to simulate driver choices in heterogeneous, weak lane discipline traffic. In contrast, [11] employs binary image processing techniques to detect vehicles in unstructured environments. However, these works focus on isolated behavior or perception modeling tasks and do not integrate these components with motion planning or control.

Across these studies, several limitations persist: lateral motion is frequently simplified or omitted; vehicle dynamics are often modeled using point-mass assumptions; and surrounding vehicles are assumed to behave predictably or follow traffic norms attributed to the low density traffic in regions with advanced transportation infrastructure. These assumptions are rendered invalid in the unstructured urban slow-moving traffic with minimal lane-discipline.

This work proposes a hybrid feedback-predictive control framework for ego-vehicle navigation in dense, unstructured traffic. The vehicle is modeled using a kinematic bicycle model, with steering and throttle as the only control degrees of freedom. The method does not rely on lane structure, formation control, or behavioral compliance from neighboring vehicles. Instead, it integrates zone-based perception, feedback stabilization, and trajectory sampling with cost-based selection, enabling responsive and feasible motion planning in environments with no structure and unpredictable behavior. The proposed reference planner computes a vitual reference lane instead of following fixed reference lanes, demonstrating adaptability to traffic characterized by low-lane discipline.

This article is organized as follows: Section II provides an overview of the proposed system, and Section III describes the vehicle model. Sections IV–VII present the core components of the control methodology, namely, perception, planning, feedback control, and optimization, in sequence. Simulation results are presented in Section VIII, and conclusions are drawn in Section IX.

II. System Overview

The proposed control framework for ego-vehicle navigation in dense, lane-less traffic consists of four interconnected modules that together enable responsive and safe motion planning:

1) **Perception Module**: Classifies neighboring vehicles into frontal, left, and right zones based on relative angle and distance. This spatial categorization forms the basis for context-aware planning and control.
2) **Reference Planner**: Computes the target velocity and virtual lane using zone-based perception. The velocity is derived from braking distance constraints and lateral steering dynamics, while the virtual lane is estimated from lateral gaps to side vehicles and road boundaries.
3) **Feedback Controller**: Implements a simple proportional-derivative (PD) control law to track the reference speed and virtual lane center. It computes steering and throttle commands based on lateral deviation, heading error, and velocity error, providing reactive stabilization and also serving as a fallback when predictive planning is infeasible.
4) **Predictive Optimizer**: Samples control inputs over a finite horizon and simulates ego trajectories using a kinematic bicycle model. Each trajectory is evaluated using a multi-term cost function that penalizes road edge violations, collisions, clearance violations, deviation from feedback commands, and abrupt changes in control inputs. The lowest-cost feasible trajectory is selected for execution.

III. Vehicle Model

The proposed framework is specifically designed for dense, lane-less traffic scenarios where vehicles operate at low speeds. Under such conditions, dynamic effects such as tire slip and friction are negligible, making the pure kinematic bicycle model a suitable choice. This model has been widely adopted in low-speed autonomous driving applications due to its geometric simplicity and computational efficiency (see, e.g., [12], [13], [14]). For mathematical modeling, the left and right wheels of both the front and rear axles are collapsed onto the vehicle's centerline, resulting in a simplified geometry that resembles a bicycle. The vehicle model is expressed as:

$$\dot{\mathbf{x}} = [v\cos(\phi) \quad v\sin(\phi) \quad \frac{v}{L}\tan(\delta) \quad a]^T \tag{1}$$

where $\mathbf{x} := [x \;\; y \;\; \phi \;\; v]^T$ is the state vector and $\mathbf{u} := [\delta \;\; a]^T$ is the control input vector. Here, (x, y) denote the vehicle's position in the global inertial frame, ϕ is the global heading angle, v is the longitudinal velocity, δ is the steering angle, a is the longitudinal acceleration (throttle input), and L is the wheelbase, see Fig. 1. The system is subject to the following fundamental constraints: $v \geq 0$ m/s, $\delta \in [\delta_{\min}, \delta_{\max}]$, and $a \in [a_{\min}, a_{\max}]$. Steering induces a lateral (centripetal) acceleration, which is bounded by $a_{\text{max,lat}}$. In addition, the vehicle's frontal and side perception ranges are denoted by d_{F} and d_{S} respectively, will be elaborated in the following section.

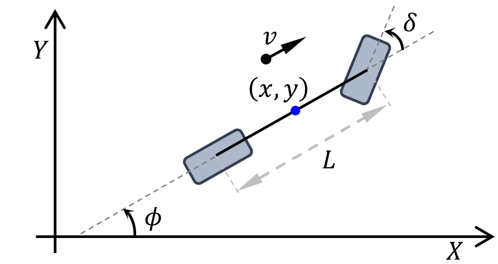

Fig. 1: Schematic of the kinematic bicycle model.

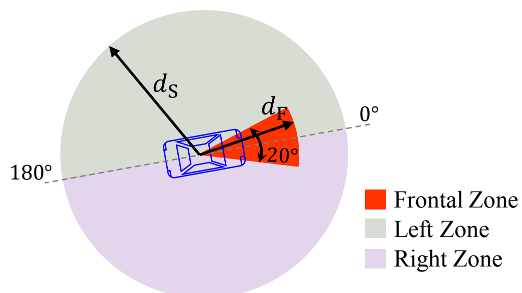

Fig. 2: Perception zones relative to the ego-vehicle.

IV. Zone-Based Perception Module

To enable context-aware planning, the ego-vehicle defines three directional zones within its fixed perception field, based on relative angle θ and distance d thresholds (see Fig. 2):

- **Frontal Zone, $\mathbf{Z}_\mathrm{F}$**: $|\theta| \leq 10°$, $d < d_\mathrm{F}$. Captures vehicles directly ahead, relevant for speed regulation and collision avoidance.
- **Left Zone, $\mathbf{Z}_\mathrm{L}$**: $0° < \theta \leq 180°$, $d < d_\mathrm{S}$. Includes vehicles to the left, used for lateral clearance and virtual lane estimation.
- **Right Zone, $\mathbf{Z}_\mathrm{R}$**: $-180° \leq \theta < 0°$, $d < d_\mathrm{S}$. Includes vehicles to the right, complementing the left zone in evaluating spatial constraints and guiding lateral motion.

Let each neighboring vehicle $i \in \mathcal{N}$ have a polygonal shape $\mathcal{P}_i \subset \mathbb{R}^2$. Then, the sets of vehicles whose shapes intersect the respective zone regions are defined as:

$$\mathcal{V}_\mathrm{F} := \{i \in \mathcal{N} \mid \mathcal{P}_i \cap \mathbf{Z}_\mathrm{F} \neq \emptyset\} \tag{2a}$$
$$\mathcal{V}_\mathrm{L} := \{i \in \mathcal{N} \mid \mathcal{P}_i \cap \mathbf{Z}_\mathrm{L} \neq \emptyset\} \tag{2b}$$
$$\mathcal{V}_\mathrm{R} := \{i \in \mathcal{N} \mid \mathcal{P}_i \cap \mathbf{Z}_\mathrm{R} \neq \emptyset\} \tag{2c}$$

where $\mathbf{Z}_\mathrm{F}$, $\mathbf{Z}_\mathrm{L}$, and $\mathbf{Z}_\mathrm{R}$ denote the spatial regions corresponding to the frontal, left, and right zones respectively, and $\mathcal{V}_\mathrm{F}$, $\mathcal{V}_\mathrm{L}$, $\mathcal{V}_\mathrm{R}$ are the corresponding sets of vehicles overlapping those regions.

Note that $d_\mathrm{F} < d_\mathrm{S}$, therefore, $\mathcal{V}_\mathrm{F} \subset (\mathcal{V}_L \cup \mathcal{V}_R)$. Vehicles may be recorded in multiple zones if they meet more than one criterion. This abstraction supports structured reasoning over unstructured traffic by simplifying spatial complexity into manageable perceptual categories, enabling responsive and context-aware control.

V. Reference Planning Module

The absence of lane markings and the lack of lane discipline on many Indian roads present a significant challenge, as conventional LKS cannot be applied in such environments. To address these challenges, the planning logic is introduced to generate intermediate motion references based on the perceived traffic configuration. The references consist of the target velocity and a virtual reference lane y_{ref}, both derived from the spatial relationships with neighboring vehicles and road boundaries. These outputs serve as reference signals for the downstream control modules, enabling structured motion planning even in unstructured traffic scenarios.

A. Reference Velocity Computation

In lane-less traffic environments, maintaining a constant preset cruise velocity can be unsafe, as the ego-vehicle must adapt its speed to ensure safe braking when frontal obstacles are encountered and also account for lateral motion during steering. To achieve this, three velocity components are considered: the nominal cruise velocity v_N; the braking velocity v_B, derived from the safe stopping distance constraint (3); and the curvature-constrained velocity v_C, which represents the maximum speed permitted by the path curvature so that lateral acceleration remains within its limit, derived from lateral acceleration limits (5). The target reference velocity v_ref (7) is then obtained using a smooth minimum operator applied to these values, ensuring responsive braking and safe turning.

When no vehicles are detected within the frontal zone, the ego-vehicle maintains a nominal cruise velocity v_N. Otherwise, the velocity is reduced to satisfy braking distance requirements, given by

$$v_\mathrm{B} = \sqrt{2\,|a_\mathrm{min}|\,\max(0, (\Delta x_\mathrm{avg} - d_\mathrm{safe}))}, \tag{3}$$

derived from the classical stopping distance kinematic relation $v_\mathrm{B}^2 = -2\,a_\mathrm{min}\,s$, with $s = \Delta x_\mathrm{avg} - d_\mathrm{safe}$, denoting the required stopping distance, where a_min represents maximum braking. This ensures that the ego-vehicle can decelerate safely to avoid collisions with frontal obstacles. In (3), the headway distances to frontal vehicles $i \in \mathcal{V}_\mathrm{F}$ are weighted by inverse distance d_i:

$$\Delta x_\mathrm{avg} = \frac{\sum_{i \in \mathcal{V}_\mathrm{F}} w_{F,i}\,\Delta x_i}{\sum_{i \in \mathcal{V}_\mathrm{F}} w_{F,i}}, \quad w_{F,i} = \frac{1}{d_i}, \tag{4}$$

Here, d_safe is the minimum stand-still headway clearance maintained by each vehicle w.r.t. their neighbors and Δx_i is the relative distance of the $i-$th vehicle to the ego-vehicle, equal to $(x_i - x)$, see Fig. 3.

Additionally, the curvature-constrained velocity v_C is adapted based on the steering output command δ, given by

$$v_\mathrm{C} = \sqrt{\frac{a_\mathrm{max,lat}\,L}{\tan(|\delta| + \varepsilon)}}, \tag{5}$$

which follows from the centripetal acceleration relation $a_\mathrm{lat} = v_C\,\dot{\phi}$ and the vehicle model (1), where a_lat

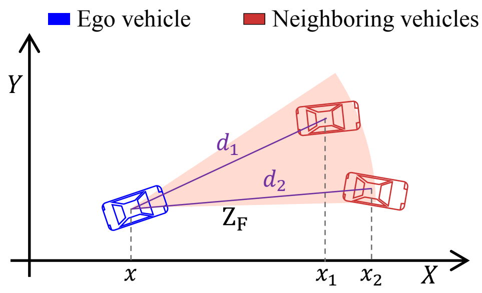

Fig. 3: Average headway computation.

denotes the lateral acceleration of the ego-vehicle . The small offset ε is introduced to avoid singularity, ensuring numerical stability during straight driving when $\delta \approx 0$.

To ensure smooth transitions between velocity modes, the smooth minimum operator $\mathrm{smin}_\epsilon(\cdot)$ is used, defined as

$$\mathrm{smin}_\epsilon(\{x_i\}_{i=1}^N) = \epsilon \log \left\{ \sum_{i=1}^{N} \exp\left(\frac{x_i}{\epsilon}\right) \right\}, \quad \epsilon < 0, \tag{6}$$

where ϵ is the smoothing parameter [15]. As $\epsilon \to 0^-$, the operator converges to the exact minimum function $\min(\cdot)$.

The final reference velocity is computed as

$$v_{\text{ref}} = \begin{cases} \mathrm{smin}_\varepsilon(v_{\text{N}}, v_{\text{C}}), & \mathcal{V}_{\text{F}} = \emptyset \\ \mathrm{smin}_\varepsilon(v_{\text{N}}, v_{\text{C}}, v_{\text{B}}), & \mathcal{V}_{\text{F}} \neq \emptyset\,. \end{cases} \tag{7}$$

B. Reference Lane Estimation

The primary challenge on many roads in emerging regions like India is the lack of lane discipline or lane markings. Therefore, relying on lane markings as a reference is not a viable option for safe autonomous driving. Inspired from [5], the reference lateral position is estimated from the spatial distribution of neighboring vehicles in the left and right zones, along with lateral road boundaries. Lateral positions are weighted by inverse distance, similar to the headway averaging in (4). The weighted averages are computed as

$$\begin{aligned} y_{L,\text{avg}} &= \frac{\left\{\sum_{i\in\mathcal{V}_{\text{L}}} w_{L,i}\,(y_i - d_o)\right\} + w_{L,e}\, y_{L,e}}{\left(\sum_{i\in\mathcal{V}_{\text{L}}} w_{L,i}\right) + w_{L,e}}, \\ w_{L,i} &= \frac{1}{d_i}, \quad w_{L,e} = \frac{1}{d_{L,e}}, \end{aligned} \tag{8}$$

$$\begin{aligned} y_{R,\text{avg}} &= \frac{\left\{\sum_{i\in\mathcal{V}_{\text{R}}} w_{R,i}\,(y_i + d_o)\right\} + w_{R,e}\, y_{R,e}}{\left(\sum_{i\in\mathcal{V}_{\text{R}}} w_{R,i}\right) + w_{R,e}}, \\ w_{R,i} &= \frac{1}{d_i}, \quad w_{R,e} = \frac{1}{d_{R,e}}\,. \end{aligned} \tag{9}$$

Fig. 4 gives a geometrical illustration of these formulations. Here, y_i is the lateral global position of the i-th vehicle within the zone, and d_o is an offset term to compensate for the vehicles' nominal width and a safe side clearance, since the lateral positions y_i's are computed from the vehicle center and does not account for width or clearance. Fig. 5 provides an illustrative sketch highlighting the significance of d_o. $y_{L,e}$ and $y_{R,e}$ denote the lateral positions of the left and right road edges also adjusted for nominal width and clearance, and $d_{L,e}$, $d_{R,e}$ are their respective shortest distances from the ego-vehicle. The virtual reference lane is then defined as

$$y_{\text{ref}} = \frac{y_{L,\text{avg}} + y_{R,\text{avg}}}{2}\,. \tag{10}$$

This virtual centerline, illustrated by the light green color line in Fig. 4, serves as the lateral reference for downstream control modules, enabling structured motion in unstructured traffic environments.

VI. Feedback Control Module

A. Controller Design

The feedback controller computes the steering and acceleration commands $(\delta,\, a)$ based on the reference speed v_{ref} and the estimated lane reference y_{ref}, as derived in the previous section.

For longitudinal control, the velocity error is defined as

$$e_v = v_{\text{ref}} - v\,, \tag{11}$$

and the feedback acceleration command is computed using a PD controller:

$$a_{\text{fb}} = K_{v,P}\, e_v + K_{v,D}\, \dot{e}_v\,, \tag{12}$$

where $K_{v,P}$ and $K_{v,D}$ are constant control gain parameters.

For lateral control, a lookahead point is projected forward to improve stabilization. The lookahead distance d_{LA} is a fixed parameter that determines how far ahead the reference point is placed. The desired heading is then computed as

$$\phi_{\text{ref}} = \tan^{-1}\left(\frac{y_{\text{ref}} - y}{d_{\text{LA}}\, \cos\phi}\right). \tag{13}$$

The lateral and heading errors are given by

$$e_{\Delta y} = y_{\text{ref}} - (y + d_{\text{LA}}\, \sin\phi) \tag{14}$$

and

$$e_\phi = \phi_{\text{ref}} - \phi\,. \tag{15}$$

Then the feedback steering command is computed as

$$\delta_{\text{fb}} = K_{\Delta y,P}\, e_{\Delta y} + K_{\Delta y,D}\, \dot{e}_{\Delta y} + K_{\phi,P}\, e_\phi + K_{\phi,D}\, \dot{e}_\phi\,. \tag{16}$$

where $K_{\Delta y,P}$, $K_{\Delta y,D}$, $K_{\phi,P}$, and $K_{\phi,D}$ are constant control gain parameters. The next subsection presents conditions for the feedback control parameters derived from local stability analysis. Since the local stability analysis guarantees stability only for small perturbations, the parameters are further tuned through simulation tests.

This feedback structure enables responsive control by continuously adapting to both spatial constraints and curvature-induced speed variations.

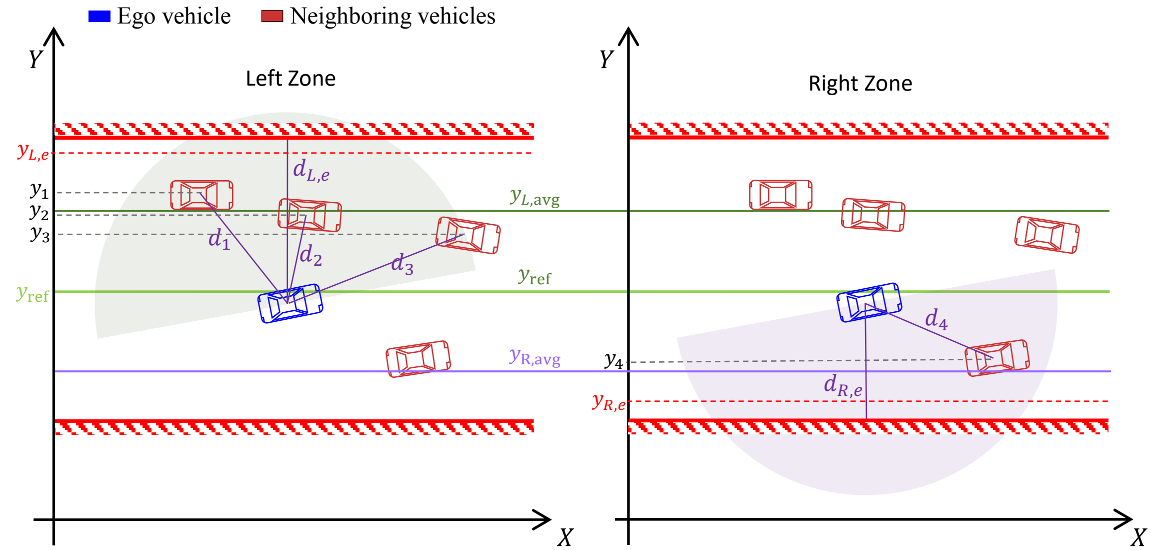

Fig. 4: Virtual reference lane estimation.

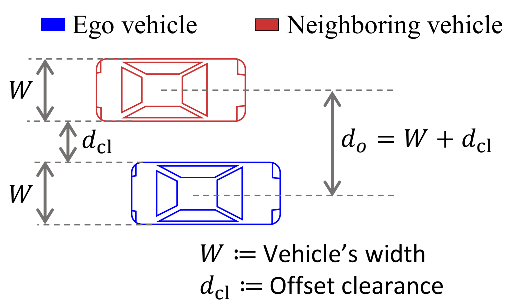

Fig. 5: Vehicle lateral geometry.

B. Local Stability Analysis

Suppose the reference signals are constant, with $v_{\text{ref}} = v^\star > 0$, $y_{\text{ref}} = y^\star$, and $\phi_{\text{ref}} = \phi^\star$. For a straight virtual reference lane, $\phi^\star = 0$. Define perturbations $\tilde{v} = v - v^\star$, $\tilde{y} = y - y^\star$, and $\tilde{\phi} = \phi - \phi^\star = \phi$.

From the longitudinal PD control law (12), the linearized closed-loop dynamics are

$$\dot{\tilde{v}} \approx -\frac{K_{v,P}}{1 + K_{D,P}}\,\tilde{v}\,. \tag{17}$$

For $K_{v,P} > 0$ and $K_{D,P} > -1$, the longitudinal subsystem is locally asymptotically stable.

Linearizing the kinematic vehicle model (1) around the equilibrium yields: $\dot{\tilde{y}} \approx v^* \tilde{\phi}$ and $\dot{\tilde{\phi}} \approx \frac{v^*}{L}\,\delta$. The lateral and heading errors (14) and (15) reduce to

$$\tilde{e}_{\Delta y} \approx -\tilde{y} - d_{\text{LA}}\,\tilde{\phi} \tag{18}$$

and

$$\tilde{e}_{\phi} \approx -\frac{1}{d_{\text{LA}}}\,\tilde{y} - \tilde{\phi}\,. \tag{19}$$

Their derivatives are

$$\dot{\tilde{e}}_{\Delta y} \approx -v^* \tilde{\phi} - \frac{d_{\text{LA}}\, v^*}{L}\,\delta \tag{20}$$

and

$$\dot{\tilde{e}}_{\phi} \approx -\frac{v^*}{d_{\text{LA}}}\,\tilde{\phi} - \frac{v^*}{L}\,\delta\,. \tag{21}$$

From the lateral PD steering law (16), the closed-loop dynamics become

$$\begin{bmatrix} \dot{\tilde{y}} \\ \dot{\tilde{\phi}} \end{bmatrix} \approx \begin{bmatrix} 0 & v^\star \\ \frac{v^\star}{L} k_1 & \frac{v^\star}{L} k_2 \end{bmatrix} \begin{bmatrix} \tilde{y} \\ \tilde{\phi} \end{bmatrix}, \tag{22}$$

where,

$$k_1 = -\frac{K_{\Delta y,P} + \frac{K_{\phi,P}}{d_{\text{LA}}}}{1 + \frac{v^\star}{L}(K_{\Delta y,D}\, d_{\text{LA}} + K_{\phi,D})} \tag{23}$$

and

$$k_2 = -\frac{K_{\Delta y,P}\, d_{\text{LA}} + K_{\phi,P} + K_{\Delta y,D} v^\star + \frac{K_{\phi,D}\, v^\star}{d_{\text{LA}}}}{1 + \frac{v^\star}{L}(K_{\Delta y,D}\, d_{\text{LA}} + K_{\phi,D})}\,. \tag{24}$$

The linearized lateral subsystem (22) is asymptotically stable if $k_1 < 0$ and $k_2 < 0$, which is ensured when all controller gains in (16) are positive, making the matrix in (22) Hurwitz.

Note that the above linearized stability proof guarantees only asymptotic convergence in the vicinity of the equilibrium. To further illustrate the stable performance, simulation results for a representative scenario are presented. A more rigorous nonlinear stability analysis would be required for a complete proof. However, given that the proposed method serves as the first structured framework in this direction, such an extension lies beyond the present scope and is left for future investigation.

VII. Predictive Optimizer Module

While the feedback controller provides reactive stabilization based on reference signals, its behavior in unstructured environments can become overly aggressive due to abrupt spatial changes and limited foresight. In such cases, relying solely on instantaneous feedback may lead to control violations such as road edge breaches, unsafe clearance, or erratic steering. To mitigate these risks, a predictive optimization layer is introduced, enabling the ego-vehicle to evaluate future trajectories over a finite horizon and select control inputs that balance feasibility, safety, and smoothness.The predictive optimizer evaluates candidate control inputs over a finite horizon using trajectory simulation and cost-based selection. It operates on the kinematic bicycle model (Section III), incorporates neighbor information detected via zone-based perception (Section IV), and penalizes deviation from feedback control (Section VI) as part of its cost function.

A. Neighbor Trajectory Prediction

For each neighbor vehicle detected within the perception zones $p \in (\mathcal{V}_L \cup \mathcal{V}_R)$, the predicted trajectory over horizon H, starting from time t, is computed under constant velocity and heading assumptions as:

$$^{p}x_{t+(h+1)\Delta t|t} = {}^{p}x_{t+h\Delta t|t} + {}^{p}v_t \cos({}^{p}\phi_t)\,\Delta t\,, \tag{25a}$$

$$^{p}y_{t+(h+1)\Delta t|t} = {}^{p}y_{t+h\Delta t|t} + {}^{p}v_t \sin({}^{p}\phi_t)\,\Delta t\,, \tag{25b}$$

where $h = 0, \ldots, H-1$, and Δt denotes sampling time of the controller. Here, ${}^{p}x_{t+h\Delta t|t}$ and ${}^{p}y_{t+h\Delta t|t}$ denote the predicted longitudinal and lateral positions of the p-th neighboring vehicle at time $t + h\Delta t$, given information available at time t. The variables ${}^{p}v_t$ and ${}^{p}\phi_t$ represent the velocity and heading angle of the p-th vehicle at time t, respectively. The notation ${}^{p}(\cdot)$ is used to distinguish the states of neighboring vehicles from those of the ego-vehicle. The iterative formulation in (25a)–(25b) thus propagates the neighbor trajectories forward under constant velocity and heading assumptions.

B. Ego-Vehicle Trajectory Sampling

Control inputs (δ_k, a_k) are uniformly sampled at discrete points within the bounded ranges $[\delta_{\min}, \delta_{\max}]$ and $[a_{\min}, a_{\max}]$. For each pair, the ego-vehicle's trajectory is simulated over horizon H, starting from time t, using the kinematic bicycle model (1):

$$x_{t+(h+1)\Delta t|t} = x_{t+h\Delta t|t} + v_{t+h\Delta t|t} \cos(\phi_{t+h\Delta t|t})\Delta t \tag{26a}$$

$$y_{t+(h+1)\Delta t|t} = y_{t+h\Delta t|t} + v_{t+h\Delta t|t} \sin(\phi_{t+h\Delta t|t})\Delta t \tag{26b}$$

$$\phi_{t+(h+1)\Delta t|t} = \phi_{t+h\Delta t|t} + \frac{v_{t+h\Delta t|t}}{L}\tan(\delta_k)\,\Delta t \tag{26c}$$

$$v_{t+(h+1)\Delta t|t} = \max(0, v_{t+h\Delta t|t} + a_k\,\Delta t)\,. \tag{26d}$$

Similar to (25), here, $h = 0, \ldots, H-1$, and Δt denotes the sampling time of the controller. The terms $x_{t+h\Delta t|t}$ and $y_{t+h\Delta t|t}$ represent the predicted longitudinal and lateral positions of the ego-vehicle at time $t + h\Delta t$, respectively, given information available at time t. The variable $\phi_{t+h\Delta t|t}$ denotes the predicted heading angle, while $v_{t+h\Delta t|t}$ denotes the predicted velocity. The parameters δ_k and a_k are the sampled steering and acceleration control inputs, respectively, applied at the k-th iteration. Finally, the operator $\max(0, \cdot)$ ensures that the predicted velocity remains non-negative.

C. Cost Evaluation

Each sampled ego trajectory is scored using a multi-term cost function:

$$J = \sum_{h=1}^{H} \left(J_{\text{rd},h} + J_{\text{col},h} + J_{\text{clr},h} + J_{\text{fb},h} + J_{\text{jrk},h} \right). \tag{27}$$

The road edge cost $J_{\text{rd},h}$ penalizes lateral deviation near the boundaries by applying inverse-square penalties as the ego-vehicle approaches the road edges:

$$J_{\text{rd},h} = \frac{w_{\text{rd}}}{(y_h - y_{R,e} + \varepsilon_1)^2} + \frac{w_{\text{rd}}}{(y_{L,e} - y_h + \varepsilon_1)^2}\,, \tag{28}$$

where w_{rd} is the weight assigned to this cost term. All weights w_* are indexed to reflect their respective cost components. Here, y_h denotes the predicted lateral position of the ego-vehicle at the h-th prediction step, while $y_{L,e}$ and $y_{R,e}$ are illustrated in Fig. 4. The inverse-square of the relative lateral distance ensures that the penalty for boundary violation increases sharply as the vehicle approaches either road edge.

The collision cost $J_{\text{col},h}$ assigns an infinite penalty if the ego-vehicle's predicted footprint intersects with any predicted footprint of the neighboring vehicle:

$$J_{\text{col},h} = \sum_{p \in (\mathcal{V}_L \cup \mathcal{V}_R)} \begin{cases} \infty, & \mathcal{P}_{\text{ego},h} \cap \mathcal{P}_{p,h} \neq \emptyset \\ 0, & \mathcal{P}_{\text{ego},h} \cap \mathcal{P}_{p,h} = \emptyset\,. \end{cases} \tag{29}$$

Here, $\mathcal{P}_{\text{ego},h}$ and $\mathcal{P}_{p,h}$ denote the polygons representing the ego-vehicle and the p-th neighboring vehicle at time step h, used for collision detection via geometric intersection. For simplicity, each vehicle is modeled as a rectangle. All $p \in (\mathcal{V}_L \cup \mathcal{V}_R)$ are fixed throughout the prediction horizon H, as these correspond to the detected vehicles from the perception module at time t. The rectangular shapes of the ego-vehicle and its neighbors are computed via coordinate transformation based on the predicted position and orientation information given by (25) and (26).

The clearance cost $J_{\text{clr},h}$ penalizes close proximity to neighboring vehicles by evaluating the minimum Euclidean distance between their boundaries:

$$J_{\text{clr},h} = \sum_{p \in (\mathcal{V}_L \cup \mathcal{V}_R)} \frac{w_{\text{clr}}}{\left(\min\limits_{u \in \partial\mathcal{P}_{\text{ego},h},\, v \in \partial\mathcal{P}_{p,h}} \|u - v\|_2 + \varepsilon_1 \right)^2} \tag{30}$$

where $\partial\mathcal{P}_{\text{ego},h}$ and $\partial\mathcal{P}_{p,h}$ are the boundaries of $\mathcal{P}_{\text{ego},h}$ and $\mathcal{P}_{p,h}$, respectively.

The feedback cost $J_{\text{fb},h}$ penalizes deviation from nominal control inputs computed by the feedback controller:

$$J_{\text{fb},h} = w_{\text{fb},1}\,(\delta_k - \delta_{\text{fb}})^2 + w_{\text{fb},2}\,(a_k - a_{\text{fb}})^2\,. \tag{31}$$

The jerk cost $J_{\text{jrk},h}$ discourages abrupt changes in control inputs $(\delta_k\,, a_k)$ relative to the previous timestep $(\delta_{\text{prev}}\,, a_{\text{prev}})$, promoting smoother actuation:

$$J_{\text{jrk},h} = w_{\text{jrk},1}\,(\delta_k - \delta_{\text{prev}})^2 + w_{\text{jrk},2}\,(a_k - a_{\text{prev}})^2\,. \tag{32}$$

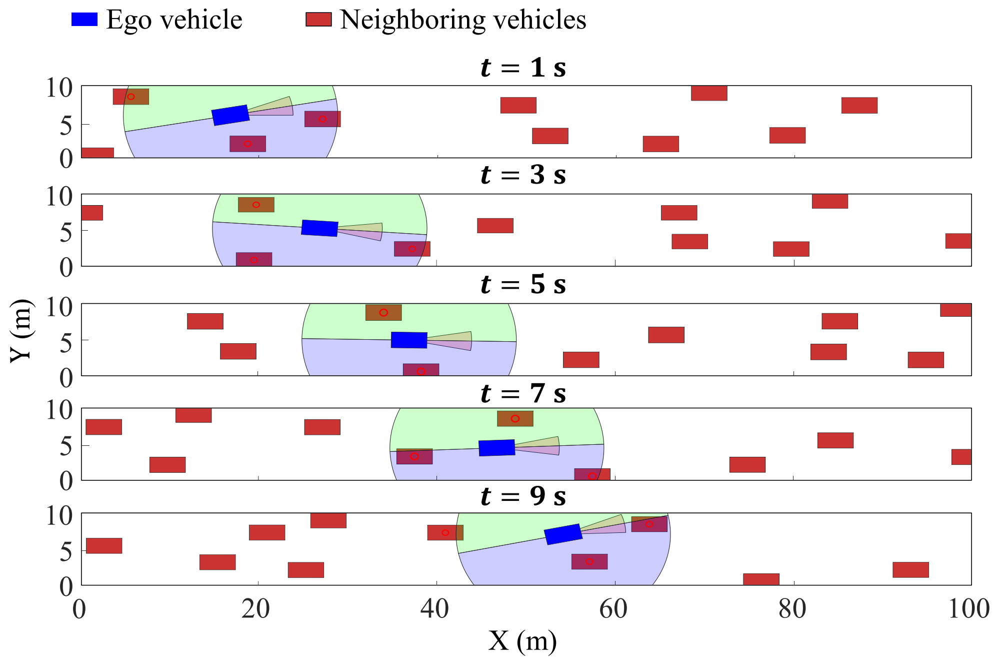

Fig. 6: Simulation snapshots illustrating ego-vehicle control in a unstructured lane-less traffic scenario.

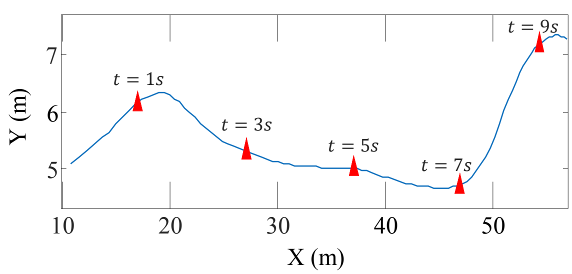

Fig. 7: Trajectory of the ego-vehicle in a representative simulation scenario over 10 s.

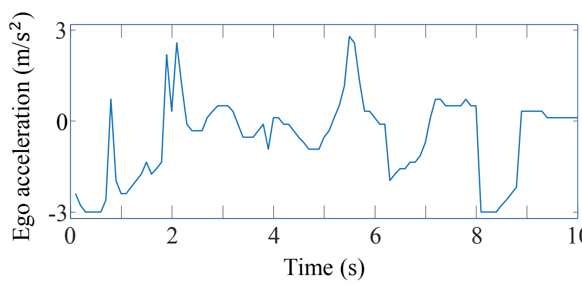

Fig. 9: Longitudinal acceleration profile of the ego-vehicle in the representative simulation scenario.

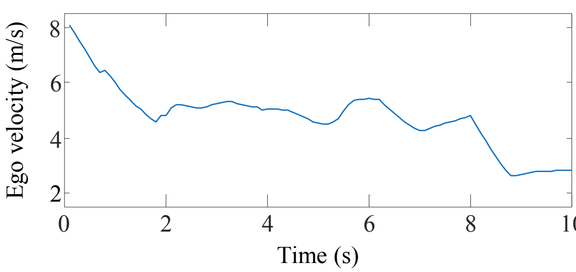

Fig. 8: Longitudinal velocity profile of the ego-vehicle in the representative simulation scenario.

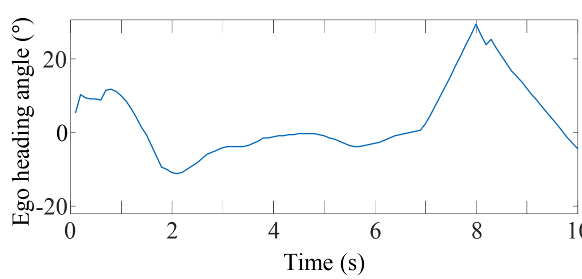

Fig. 10: Heading angle profile of the ego-vehicle in the representative simulation scenario..

VIII. Simulation Experiments

The simulation is conducted on a one-way lane that is 10 m wide, with 10 neighboring vehicles randomly spawned across the region at each initialization. The nominal speed of the neighboring vehicles is set to 8.33 m/s ($\approx$ 30 km/h), with small random deviations. Key simulation parameters are listed in Table I. Note that, the acceleration is within the range specified by ISO norm [16]. The simulation yields promising results, with the ego-vehicle successfully avoiding collisions even under severe conditions. While unstructured traffic environments can present a wide variety of scenarios, one representative case is presented here. Fig. 6 shows

TABLE I: Simulation Parameters

Parameters	Value	Unit
Δt	0.1	s
$\delta_{\min}$	$-\pi/12$	radian
$\delta_{\max}$	$\pi/12$	radian
$a_{\min}$	-3	m/s^2
$a_{\max}$	3	m/s^2
$a_{\max,\text{lat}}$	1	m/s^2
L	2.5	m
d_F	7	m
d_S	12	m
H	1	s

snapshots of the simulation at different times during the 10s runtime. Fig. 7 depicts the corresponding trajectory of the ego-vehicle, with time markers aligned to Fig. 6. Figs. 8–10 present the velocity, acceleration, and heading profiles of the ego-vehicle, demonstrating smooth and safe control performance despite the presence of unpredictable neighbors.

IX. Conclusion

This paper presented a feedback-predictive control framework for autonomous driving in unstructured lane-less traffic. The system combines zone-based perception with a dual-layer control strategy. The feedback controller reacts quickly to spatial changes, while the predictive optimizer makes more cautious decisions by evaluating future trajectories. Simulation results show that the ego-vehicle can avoid collisions and maintain smooth motion in dense, unpredictable traffic, across a wide range of challenging scenarios.

Future work will address several current limitations of the proposed framework. The stability analysis, which is presently restricted to linearized proofs, will be extended toward more rigorous nonlinear guarantees for the ego-vehicle. Neighboring vehicles in the simulations will be modeled with realistic driver behavior to better capture the nuances of Indian and similar traffic scenarios. Control parameter tuning and cost-function weighting, which are currently based on heuristic choices, could be adapted through systematic strategies to improve responsiveness across varying traffic densities. In addition, evaluation from simulation tests will be strengthened by defining and measuring key performance indicators, and later extended to testing in high-fidelity simulators such as CARLA.

References

[1] L. Masello, G. Castignani, B. Sheehan, F. Murphy, and K. McDonnell, "On the road safety benefits of advanced driver assistance systems in different driving contexts," Transportation research interdisciplinary perspectives, vol. 15, pp. 1–20, 2022.

[2] R. Rajamani, Vehicle dynamics and control. Springer Science & Business Media, 2012.

[3] P. Khound, P. Will, A. Tordeux, and F. Gronwald, "Unified framework for over-damped string stable adaptive cruise control systems," Transportation research part C: emerging technologies, vol. 148, pp. 1–24, 2023.

[4] V. Papathanasopoulou and C. Antoniou, "Flexible car–following models for mixed traffic and weak lane–discipline conditions," European transport research review, vol. 10, no. 2, p. 62, 2018.

[5] A. K. Mulla, A. Joshi, R. Chavan, D. Chakraborty, and D. Manjunath, "A microscopic model for lane-less traffic," IEEE Transactions on Control of Network Systems, vol. 6, no. 1, pp. 415–428, 2019.

[6] S. Singh, "Critical reasons for crashes investigated in the national motor vehicle crash causation survey," Tech. Rep., 2015.

[7] M. Papageorgiou, K.-S. Mountakis, I. Karafyllis, I. Papamichail, and Y. Wang, "Lane-free artificial-fluid concept for vehicular traffic," Proceedings of the IEEE, vol. 109, no. 2, pp. 114–121, 2021.

[8] A. Nagahama, A. Tomoeda, and T. Wada, "Effect of response time distribution in weak lane discipline on linear stability," Collective Dynamics, vol. 10, pp. 1–32, 2025.

[9] M. Tobisawa, K. Matsuda, T. Suzuki, T. Harada, J. Hoshino, Y. Itoh, K. Kumagae, J. Matsuoka, and K. Hattori, "Reinforcement learning-based autonomous driving control for efficient road utilization in lane-less environments," Artificial Life and Robotics, vol. 30, no. 2, pp. 276–288, 2025.

[10] A. K. Budhkar and A. K. Maurya, "Overtaking decision modeling in heterogeneous, weak lane discipline traffic," Journal of the Eastern Asia Society for Transportation Studies, vol. 12, pp. 1740–1754, 2017.

[11] G. Satyanarayana, S. Majhi, and S. K. Das, "A vehicle detection technique using binary images for heterogeneous and lane-less traffic," IEEE Transactions on Instrumentation and Measurement, vol. 70, pp. 1–14, 2021.

[12] V. Freire and X. Xu, "Optimal control for kinematic bicycle model with continuous-time safety guarantees: A sequential second-order cone programming approach," IEEE Robotics and Automation Letters, vol. 7, no. 4, pp. 11 681–11 688, 2022.

[13] J. Matute, S. Diaz, and A. Karimoddini, "Sliding mode control for robust path tracking of automated vehicles in rural environments," IEEE Open Journal of Vehicular Technology, 2024.

[14] Q. Chen, S. Wang, B. Gao, Z. Zhan, and R. Zhong, "Robust longitudinal and lateral control for mixed-vehicular platoons with string stability guarantees," Nonlinear Dynamics, pp. 1–23, 2025.

[15] P. Blanchard, D. J. Higham, and N. J. Higham, "Accurately computing the log-sum-exp and softmax functions," IMA Journal of Numerical Analysis, vol. 41, no. 4, pp. 2311–2330, 2021.

[16] K. N. De Winkel, T. Irmak, R. Happee, and B. Shyrokau, "Standards for passenger comfort in automated vehicles: Acceleration and jerk," Applied Ergonomics, vol. 106, pp. 1–9, 2023.